Available online at www.sciencedirect.com
ScienceDirect
Journal of Power Sources 178 (2008) 499–509
JOURNAL OF POWER SOURCES
www.elsevier.com/locate/jpowsour

Short-side-chain proton conducting perfluorosulfonic acid ionomers: Why they perform better in PEM fuel cells☆

K.D. Kreuer[a,*], M. Schuster[b], B. Obliers[a], O. Diat[c], U. Traub[a], A. Fuchs[a], U. Klock[a], S.J. Paddison[d], J. Maier[a]

[a] *Max-Planck-Institut für Festkörperforschung, Heisenbergstraße 1, D-70565 Stuttgart, Germany*
[b] *FuMATech, Am Grubenstollen 11, D-66386 St. Ingbert, Germany*
[c] *UMR 5819 SPrAM, CEA-CNRS-University J. Fourier, CEA-Grenoble, F-38054 Grenoble Cedex 9, France*
[d] *Department of Chemical & Biomolecular Engineering, University of Tennessee, Knoxville, Tennessee 37996, USA*

Received 28 August 2007; received in revised form 2 November 2007; accepted 5 November 2007
Available online 13 November 2007

Abstract

Short-side-chain (SSC) perfluorosulfonic acid ionomers of different ion exchange capacity, IEC, (Dow 840 and Dow 1150) are characterized with respect to water sorption, transport (proton conductivity, electroosmotic water drag and water diffusion), microstructure and visco-elastic properties as a function of temperature and degree of hydration. The data are compared to those of Nafion 117 (Nafion 1100), and the implications for the use of such ionomers as separator materials in direct methanol and hydrogen fuel cells are discussed. For this purpose, a scheme is used which allows for the simulation of the water distribution and the resulting solvent (water, methanol) fluxes and potential losses across the membranes under transient and steady state conditions. The lower solvent (water, methanol) transport across Dow 1150 in direct methanol fuel cells is essentially the result of the reduced swelling. The smaller potential losses across Dow 840 compared to Nafion 117 in hydrogen fuel cells is mainly the result of the higher charge carrier concentration. The present comparison demonstrates that combining high IEC with high mechanical stability, e.g. by increasing crystallinity as in the present case, or by increasing molecular weight, cross-linking or introducing interacting particles, results in an increase in proton conductivity and lower electroosmotic drag of water. The improved stability is also anticipated to preserve the morphology of the membrane/electrode interface under conditions at which Nafion 117 starts to show plastic deformation. Hence, this may prove to be a suitable approach to improve membrane performance in both direct methanol and PEM fuel cells.
© 2007 Elsevier B.V. All rights reserved.

Keywords: Proton conductivity; Water transport; Dow membrane; Hyflon ion; PEM fuel cell; Simulation

1. Introduction

Perfluorosulfonic acid ionomers, such as Nafion®, are commonly employed as the electrolyte in proton exchange membrane (PEM) fuel cells. They consist of a polytetrafluoroethylene (PTFE) backbone and double ether perfluoro side chains terminating in a sulfonic acid group. Another PTFE membrane, originally synthesized by the Dow Chemical Company, is a short-side-chain (SSC) version of Nafion with simpler $–OCF_2CF_2SO_3H$ pendant side chains each consisting of two C-atoms compared to four C-atoms in the case of Nafion. Although superior performance had been reported for SSC type membranes [1], there was never commercialization of this promising membrane material by the Dow Chemical Company. It was only recently that research on SSC perfluorinated ionomers experienced a renaissance, which seems to do with the accessibility of a much simpler route for the synthesis of the base monomer. Ionomers of different equivalent weight are now commercially made by Solvay Solexis under the trade name Hyflon Ion®, and initial reports on this interesting material demonstrate similar properties to the original membranes made by the Dow Chemical Company [2,3]. These include the thermal, visco-elastic (mechanical) and water absorption properties of Hyflon. Similar to the Dow membrane, the results essentially reflect the higher crystallinity (i.e. melting enthalpy) and glass transition

☆ On the occasion of Bruno Scrosati's 70th birthday.
* Corresponding author.
E-mail address: kreuer@fkf.mpg.de (K.D. Kreuer).

0378-7753/$ – see front matter © 2007 Elsevier B.V. All rights reserved.
doi:10.1016/j.jpowsour.2007.11.011

temperature when compared to Nafion. Although these properties likely depend on the membrane preparation conditions, as they due for Nafion (e.g. extrusion versus casting, choice of solvent, thermal post-treatment), the general trends seem to be a characteristic of SSC perfluorosulfonic acid ionomers. The comprehensive work of Tant et al. [4,5] on Dow membranes of different equivalent weight (EW) revealed that some crystallinity remains even for EWs below 800 g eq.$^{-1}$ where Nafion membranes are usually amorphous. Moore and Martin related the lower liquid water uptake of the Na^+-form of the SSC ionomer to its higher crystallinity [6], and work of Eisman [7] on the acid form already demonstrated, for a given EW (or ion exchange capacity, IEC), a lower proton conductivity of the SSC ionomer compared to Nafion. The conductivity of the Dow membrane of an EW of 900 g eq^{-1} was actually found to be similar to the conductivity of the commonly used Nafion membrane (EW = 1100 g eq.$^{-1}$), and glass transition temperatures around $T_g = 165\,^{\circ}C$ are reported, while that of Nafion was measured to be $T_g = 110\,^{\circ}C$. Later Eisman also reported better performance of the Dow membrane (EW = 800 g eq.$^{-1}$, thickness = 130 μm) compared to Nafion 117 membrane (EW = 1100 g eq.$^{-1}$, thickness = 175 μm) [8].

Recently, extensive first principles based molecular-level modelling studies have been undertaken on the SSC membrane [9–12]. These investigations on small (i.e. two and three repeat units) oligomeric fragments have shown how the side-chain separation and the conformations of backbone and side-chain effect preferential hydration, connectivity, water binding, and proton dissociation under minimal hydration conditions (i.e. 1–3 H_2O/–SO_3H).

There is, however, no consistent understanding of the well established performance improvement of the SSC membrane, and we have therefore decided to carefully study the water sorption, transport and visco-elastic properties of four different EW (nominally 800, 840, 900 and 1150 g eq.$^{-1}$) SSC membranes and to discuss the implications on their performance in PEM fuel cells. We have developed a scheme, for the latter, which allows us to simulate the water distribution and the resulting resistance of membranes under transient and steady state conditions.

2. Experimental

The SSC *membranes* used for this study were Dow membranes of various equivalent weights, which were determined by titration and NMR. Samples of the membranes were immersed in 1 M NaCl solution for one day and then titrated with 0.1 M NaOH (Mettler Titrator DL21). The samples (in their Na^+ form) were dried (after titration) in a vacuum oven at $T = 140\,^{\circ}C$. Residual water was determined by NMR. The ion exchange capacities were determined to be 1.22, 1.16, 0.97 and 0.93 meq. g^{-1} corresponding to equivalent weights of 836, 858, 1033 and 1084 g eq.$^{-1}$. In the following, the latter will be used to distinguish the specific membrane (e.g. Dow 858). Since the IEC are close for the membranes with the lowest and highest values, most measurements have been restricted to Dow 858 (thickness ≈80 μm) and Dow 1084 (thickness ≈90 μm). Nafion 117 (EW = 1100 g eq.$^{-1}$, thickness ≈120 μm) was also included in this study for comparative purposes. The acronym Nafion 1100 is used through out to be consistent with nomenclature. Prior to all measurements, the membranes were preconditioned by leaving them in a 1 M aqueous solution of nitric acid at $T = 60\,^{\circ}C$ before carefully washing them in double distilled water at the same temperature. This standardization appeared to be essential for obtaining reproducible results, e.g. drying Nafion severely reducing its swelling capability and even leaving standardized Nafion in water at room temperature reduced its water content, while this effect is hardly observable for the Dow membrane samples.

2.1. Water hydration isotherms

Water hydration isotherms at room temperature were determined by equilibrating the membrane samples in a desicator purged with nitrogen gas of predefined relative humidity. Relative humidities were changed from high to low and from low to high values, which resulted into somewhat different degrees of hydration (the observed hysteresis were significantly more pronounced for Nafion compared to Dow membranes). The hydration levels were determined by weighing on an external balance and comparing the weight to that of the dried membrane ($T = 140\,^{\circ}C$, vacuum).

2.2. Water hydration isobars

Water hydration isobars were determined by thermogravimetric analysis (TGA) at a water partial pressure of $p_{H_2O} = 10^5$ Pa (1 atm) and temperatures ranging from $T = 105$–$180\,^{\circ}C$. A Mettler AT20 balance was magnetically coupled (Rubotherm) to the sample, which allowed measurements under high humidity conditions without condensation of water in the balance. Water was injected into the system by a peristaltic pump (Ismatec) via a pre-vaporizer in order to avoid fluctuations in the pressure. Heating and cooling rates were both keep constant at $0.2\,^{\circ}C\,min^{-1}$.

2.3. Swelling

Swelling in water was determined as a function of temperature by immersing the membranes (approximately 200 mg) in double distilled water for 2 h. For temperatures above $T = 100\,^{\circ}C$ stainless steel autoclaves were used to prevent the water from evaporating. The liquid water on the surface of the wet membranes was quickly removed using tissue paper before weighing. Finally the weight of the dry membrane was obtained by drying the membrane at $T = 140\,^{\circ}C$ in a vacuum oven.

Swelling at room temperature was also determined as a function of pre-treatment at temperatures up to $T = 150\,^{\circ}C$ for 2 h in a stream of pure nitrogen equilibrated with water at room temperature ($p_{H_2O} = 17$ hPa). While the membrane samples were free of any stress in this set of experiments, a pressure ($p = 130$ MPa) was applied to wet membranes in an open press between heated Teflon plates for periods of 30 min at different temperatures before measuring the water uptake at room temperature.

2.4. Small angle X-ray scattering (SAXS)

Small angle X-ray scattering (SAXS) was carried out on a home-built camera using an FR591 Nonius rotating Cu anode operating with a fine focus at a 6° takeoff angle corresponding to a 0.2 mm × 0.2 mm apparent beam size. The beam was K_α/K_β filtered (wavelength Cu Kα: λ = 1.5418 Å) and focused in horizontal and vertical directions by total reflection from two curved Franks mirrors (Ni-coated glass optical flats). Scattering patterns were recorded with a two-dimensional position-sensitive gas-filled detector. The sample detector distance was placed at 1 and 3.5 m to explore q values from about $q = 0.01$ up to 0.3 $Å^{-1}$ where q is the momentum transfer ($q = (4\pi \sin\theta/\lambda)$) and 2θ the total scattering angle. The sample-detector distance was calibrated using silver as a standard. The normalization of the scattering data was applied by first measuring the transmission with a semi-transparent beam stop, followed by the thickness of each sample, and finally using a Lupolen sample as a calibrating sample [13]. The samples (2 or 3 pieces for a total of about 300–500 μm thick) were placed in a brass cell between 2 thin sheets of Mylar.

2.5. Dynamic mechanical analysis (DMA)

Dynamic mechanical analysis (DMA) were performed on a Triton DMA analyzer (Tritec 2000) as a function of temperature and fixed relative humidity. The temperature and water partial pressure for each measurement were kept constant for at least 1 h. The maximum elongation was 0.01 mm at a frequency of 1 Hz (sample dimensions typically in the range of 4 mm × 5 mm × 0.05–0.2 mm).

2.6. Proton conductivities

Proton conductivities were derived from ac-impedance spectra of a two-electrode arrangement measured by an HP-ac-impedance analyzer (4192A LF) in the frequency range from 10 to 10 MHz with an oscillating voltage of 0.1 V. The measurements were performed in a closed cell with pre-equilibrated samples (10–30 stacked slices of each membrane with pre-adjusted water content, diameter ∼6 mm, thickness 2–5 mm) with gold electrodes. In this way, conductivities as a function of temperature but for a constant degree of hydration (λ = constant) have been measured.

In-plane conductivities as a function of relative humidity were also determined by four-probe impedance measurements. The cell consists of two connected compartments, each held at a different temperature. The cold compartment contained liquid water, while the hot chamber hosted the membrane under test. The relative humidities were calculated from the ratio of the saturated water vapor pressures at the temperatures of the cold and hot compartment.

Conductivity measurements in pure water vapor ($p_{H_2O} = 10^5$ Pa) were carried out in a double wall temperature controlled glass chamber with an open outlet at temperatures between $T = 110$ and 160 °C. Liquid water was continuously evaporated by a heater and injected into the chamber with a constant flow rate using a digital peristaltic pump (Ismatec). Inside the chamber the membranes (10–20 staged slices of membranes with diameter 8 mm and total thickness of 2–4 mm) were placed in a porous cylindrical tube with a gold electrode at the bottom. The second gold electrode was pressed from the top onto the stack of membranes by a screw in order to assure optimum contact. The measured sample resistance was found to be independent of the contact pressure for all stacked-slices sample geometries inferring that there was no significant contribution due to contact resistance.

Specific conductivities were obtained from the high-frequency intercept of the complex impedance with the real axis and the dimensions of the stacks. The proton conductivity diffusion coefficients, D_σ, were obtained from conductivity data σ using the Nernst–Einstein relation:

$$D_\sigma = \frac{RT\sigma}{F^2 c_{H^+}}$$

where T, R, and F have their usual meaning. The concentration of protonic charge carriers, c_{H^+}, is readily calculated from the IEC (assuming full dissociation) and the volume changes associated with the swelling.

2.7. Water diffusion coefficients

Water diffusion coefficients were determined by the pulsed magnetic field gradient NMR technique using a home built spectrometer [14] operating at a resonance frequency of $\nu = 50$ MHz and magnetic field gradients of the order $G = 10^{-2}$ T cm^{-1}. Membrane stacks of defined water contents were sealed into glass tubes positioned within the rf coil. The same spectrometer was used for the measurement of electroosmotic drag coefficients [15] by passing protonic currents through the samples using standard carbon electrodes with a Pt loading of 1 mg cm^{-2}.

3. Results and discussion

3.1. Membrane properties

A general problem in the development of sulfonic acid based ionomers is the trade off between high IEC and acceptable viscoelastic properties: with increased IEC, such ionomers tend to soften or even dissolve in the presence of water. The commonly used Nafion with an equivalent weight of 1100 g $eq.^{-1}$ (0.91 meq. g^{-1}) reflects such a compromise. The comparison of the hydration isotherms of Nafion 1100 and Dow membranes of different equivalent weight at room temperature (Fig. 1) already suggests that this compromise may be at a higher IEC for the SSC ionomer. Dow 1084, which has about the same IEC as Nafion 1100, shows similar hydration over the whole relative humidity range. But in liquid water, the water uptake of Dow 1084 is only λ = 12 compared to λ = 20 for Nafion (Fig. 2). Dow 858, which has an IEC almost 30% higher than Nafion 1100, shows higher hydration especially in the range RH = 70–100%, where the elastic properties of the membranes are mainly determining the water uptake. But in liquid water, the hydration appears to be almost identical to that of Nafion 1100 (λ = 22 compared

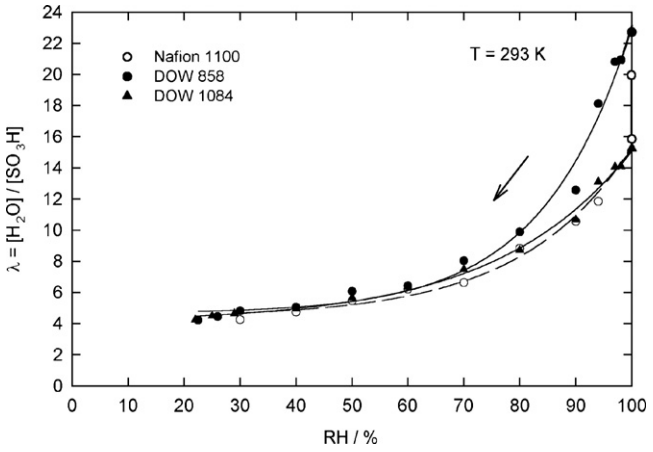

Fig. 1. Hydration isotherms recorded at room temperature ($T = 293\,^{\circ}$K) for Nafion 1100 and two Dow membranes of different equivalent weight**.** In all cases similar hysteresis is observed, but for the reason of clarity, only the data of the runs from higher to lower relative humidity are shown.

to $\lambda = 20$). But one should keep in mind that the 30% higher water volume fraction simply reflects the difference in the IEC. It should also be noted that for all membranes water sorption and swelling is dependent on the history of the sample, where time, temperature, and relative humidity are the determining factors. It is a general observation from this study that these factors are more pronounced for Nafion than for the Dow membranes.

The increase in swelling with increasing temperature is also distinctly different for Nafion than for Dow. While swelling of Nafion 1100 is virtually constant up to about $T = 140\,^{\circ}$C, where exaggerated swelling abruptly begins (for a swelling time of 1 h), the swelling of Dow membranes gradually increases with temperature, especially for Dow 1084 no exaggerated swelling is observed up to $T = 160\,^{\circ}$C (Fig. 2).

As pointed out earlier [2–5] this behavior is probably the consequence of a higher glass transition temperature and crystallinity in the SSC membrane. Even in the SAXS spectrum the latter is indicated as a broad peak in the range $q = 0.03$–0.07 Å^{-1}

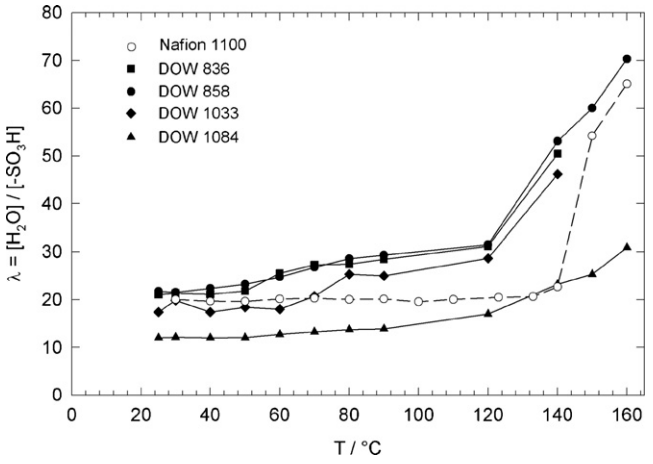

Fig. 2. Swelling of Nafion and Dow membranes of different equivalent weight as a function of temperature. Note that the membrane pieces were free of any stress and strain during the swelling process. One may also compare the data to these shown in Fig. 12.

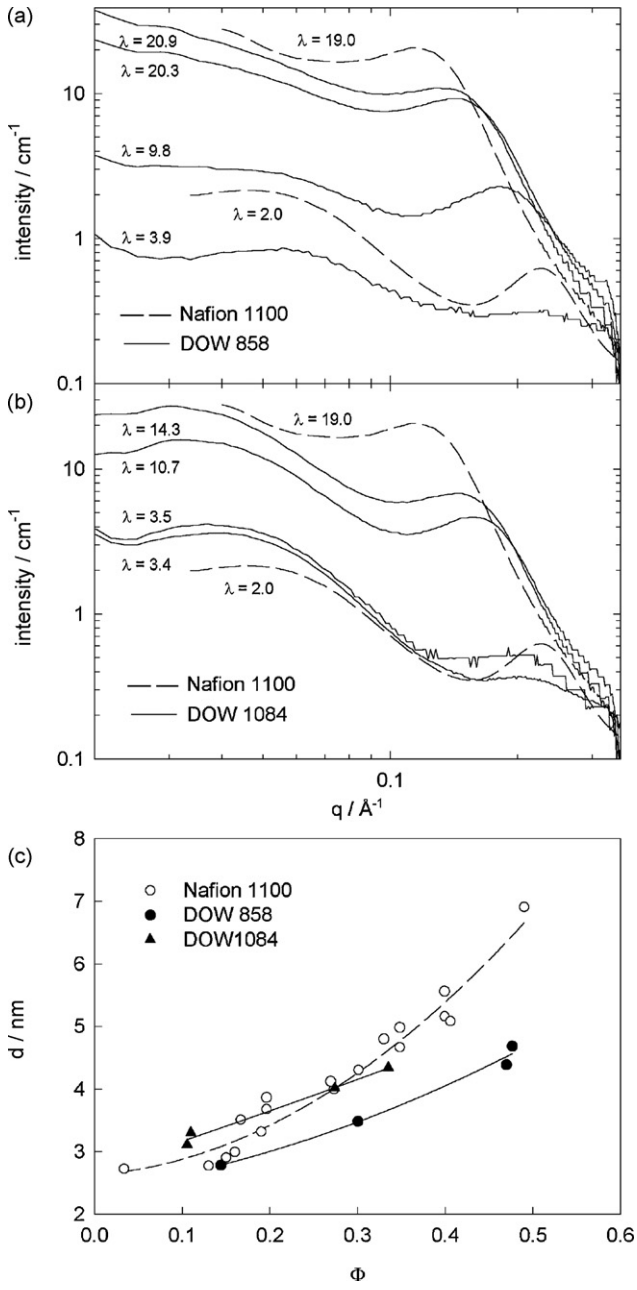

Fig. 3. (a and b) Small angle X-ray diffraction spectra (SAXS) for Dow 858 and Dow 1084 membranes, respectively, as a function of the degree of hydration. A spectrum of Nafion 1100 for selected degrees of hydration is shown for comparison. Note that the ionomer peak is more pronounced for Nafion (smaller width and higher intensity) with a position at lower momentum transfer. (c) Average hydrophobic/hydrophilic separations (spacing) as obtained from the position of the ionomer peaks. Note that the data are plotted as a function of the water volume fraction; all data virtually fall onto one curve for a plot versus $\lambda = [H_2O]/[-SO_3H]$ (not shown).

(Fig. 3b). For Dow 1084 this scattering contribution is higher than for Nafion 1100 for a given water volume fraction. However, for Dow 858 this scattering is visible only at low water contents (Fig. 3a), i.e. this is the IEC range, at which the SSC ionomer begins to lose its crystallinity. Of course, melting enthalpies obtained by DSC, provide more quantitative information on the degree of crystallinity [3], which also depends on the membrane

pre-treatment. But SAXS data give quite reliable information on the hydrophobic/hydrophilic separation in the amorphous part of the ionomer. The typical separation length and distribution is readily obtained from the position and width of the ionomer peak. The ionomer peak for the Dow membranes is generally broader than for Nafion, and its position is less dependent on the water volume fraction (in Fig. 3 we have chosen water volume fractions φ instead of hydration numbers λ to allow comparison of the scattering curves of ionomers with different IEC). In other words, there is less periodicity in the hydrophilic/hydrophobic sequence and less pronounced separation with increasing water content. This behavior is reminiscent of hydrocarbon membranes [16], and clearly indicates a higher rigidity of the SSC ionomer microstructure compared to the structure of the long side-chain variety (Nafion). The average hydrophilic/hydrophobic separation as a function of the water volume fraction (Fig. 3c) actually shows distinct differences between Nafion 1100 and Dow 858. Especially at high water contents, separation is more developed in Nafion 1100 than in Dow 858. This also implies that the average width of the hydrated hydrophilic channels is smaller for the Dow membranes, at least for medium and high water contents [17]. Only at low water contents, does the rigidity of the Dow microstructure seem to preserve the structural features attained at medium degrees of hydration; e.g. the typical separation length for Dow 1084 is slightly higher than for Nafion 1100 at water contents below about $\varphi = 10\%$.

These microstructural features have consequences for the transport of water and protonic charge carriers within the hydrated hydrophilic domain [16,17]. Surprisingly, the water diffusion coefficient is virtually identical for all three membranes at very high water contents ($\varphi > 30\%$ which corresponds to $\lambda > 15$–20, Fig. 4a). For decreasing hydration, however, the water diffusion coefficient of the Dow membranes decreases more than that observed for Nafion 1100 (Fig. 4a). In the case of Dow 858, this may also be the consequence of its higher IEC (a similar trend for the transport in poly-arylenes of different IEC has been explained by the increasing water volume fraction involved in the solvation of the sulfonic acid groups [18]). For Dow 1084, however, this most likely reflects a microstructure, which less effectively adjusts to low water contents. In this respect, the high flexibility of the long side-chain architecture of Nafion appears to be more favorable for accommodating well-connected water structures even at very low degrees of hydration. This behavior is also reflected in the activation enthalpy of water diffusion (Fig. 4b): this is lowest for Nafion 1100 in the entire hydration range, only for very high hydration levels, all data approach that of pure water ($E_a = 0.17$ eV).

As is the case for all hydrated sulfonic acid ionomers, the proton conductivity diffusion coefficient D_σ (mobility of protonic defects) closely follows the water diffusion coefficient (Fig. 5), especially at low degrees of hydration, where proton transport is essentially vehicular [19], i.e. hydronium ion transport in an aqueous environment. Only at high hydration levels is there the usual contribution from structure diffusion as indicated by $D_\sigma > D_{H_2O}$. As for the water diffusion coefficient, values for D_σ are very close for all three ionomers at high degrees of hydra-

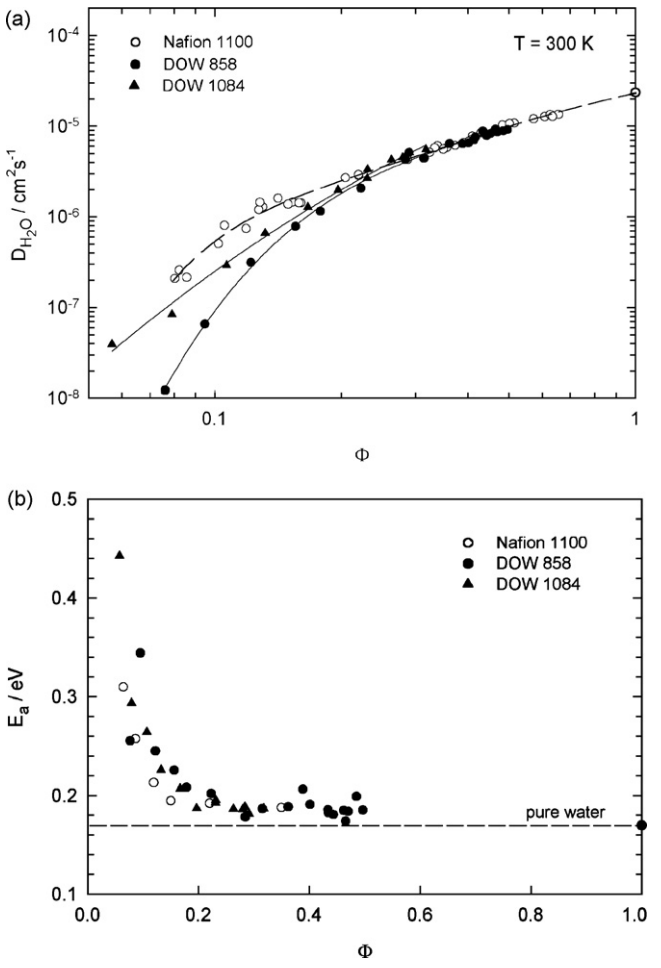

Fig. 4. (a) Room temperature water diffusion coefficient for Dow 858 and Dow 1084 as a function of the water volume fraction φ as obtained by PFG-NMR. (b) Activation enthalpy of water diffusion as obtained from the temperature dependence of the water diffusion coefficient in the range $T = 25$–$80\,^\circ$C. With increasing water content, the data approach the value of the activation enthalpy of self-diffusion in pure water (dashed line). The corresponding data for Nafion 1100 are shown for comparison.

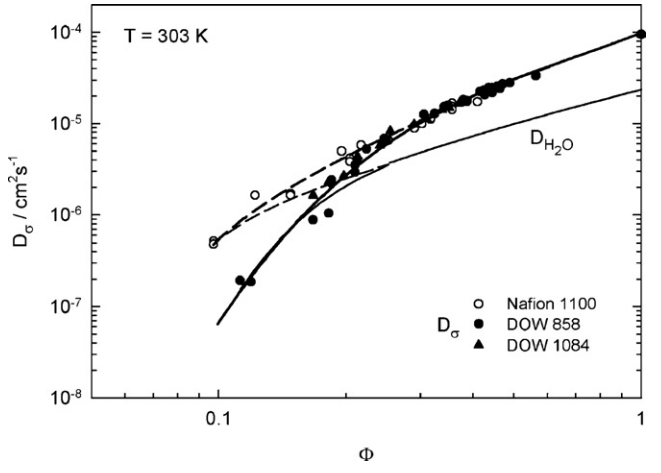

Fig. 5. Conductivity diffusion coefficient D_σ for Dow 858, Dow 1084 and Nafion 1100 as a function of the water volume fraction φ. The corresponding water diffusion coefficients are shown for comparison.

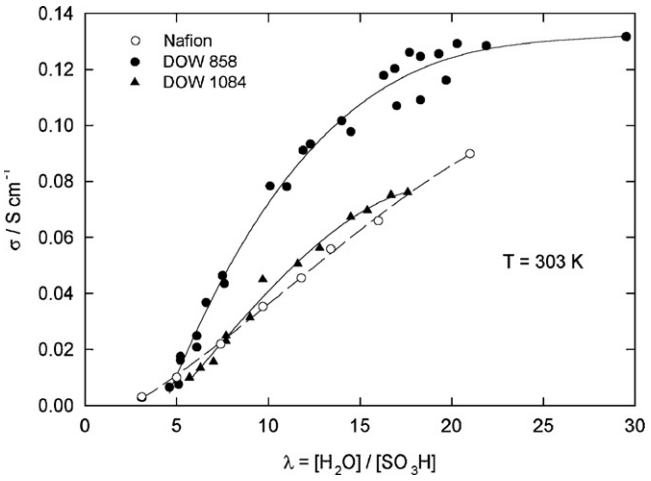

Fig. 6. Room temperature proton conductivity of Dow 858 and Dow 1084 as a function of $\lambda = [H_2O]/[-SO_3H]$. The corresponding data for Nafion 1100 are shown for comparison.

tion. Considering the microstructural differences especially at high water contents (see above and Fig. 3), this is surprising. Obviously, there is something about the microstructure of SSC ionomers at high levels of hydration which allows for high water diffusion and proton mobility despite the lower degrees of hydrophobic/hydrophilic separation (Fig. 3) and higher IEC in the case of Dow 858 (charge carrier concentration). This high proton mobility is part of the very high room temperature proton conductivity especially of Dow 858, which is shown in Fig. 6 as a function of λ. Since the hydration isotherms of Dow 858 and Nafion 1100 are almost identical (Fig. 1), λ can be taken as a measure of the relative humidity, i.e. for a given relative humidity the room temperature proton conductivity of Dow 858 is almost 50% higher than that of Nafion 1100. With similar proton mobilities D_σ for a given water volume fraction, this difference is then the effect of the higher charge carrier concentration (i.e. IEC) and the higher water volume fraction which leads to an increased water diffusion coefficient (Fig. 4) and proton mobility (Fig. 5).

With increasing temperature the conductivity of Dow 858 remains higher than this of Nafion 1100. For a constant water partial pressure of $p_{H_2O} = 10^5$ Pa (1 atm), which is typical for fuel cell applications, the conductivity of both Dow membranes is decreasing less with temperature than the conductivity of Nafion 1100 (Fig. 7). This leads to a further increase of the conductivity difference especially for Dow 858 and Nafion, which amounts to a factor of two for temperatures near $T = 150\,^\circ$C (i.e. 7 mS compared to 3.5 mS). This is not a large effect (especially when considering error bars of about 20%), but it is significant and not anticipated from the room temperature behavior. The relative humidity is already quite low in this temperature regime (RH ∼ 20%, λ ∼ 2.5 according to Fig. 8) and the corresponding water volume fraction is far below $\varphi = 0.1$. At such low water contents, the room temperature proton conductivity of the SSC ionomers is already lower than the conductivity of Nafion 1100 (see Figs. 5 and 6 and discussion above). At higher temperatures, this is no longer the case, i.e. the conductivity of Dow 858 remains higher than the conductivity of Nafion 1100 also at

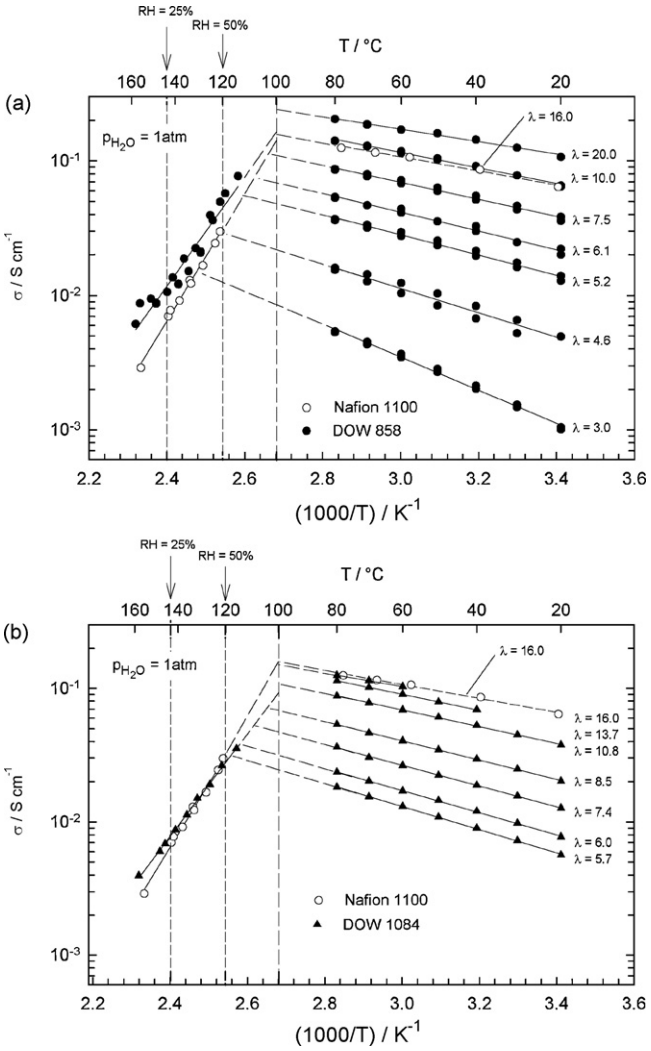

Fig. 7. Proton conductivities of Dow 858 (a) and Dow 1084 (b) as a function of temperature ($T = 25$–$80\,^\circ$C) for different water contents $\lambda = [H_2O]/[-SO_3H]$. Dashed lines are extrapolations to the conductivity measured at a constant water pressure of $p_{H_2O} = 10^5$ Pa (1 atm). The corresponding conductivity of Nafion 1100 is shown for comparison.

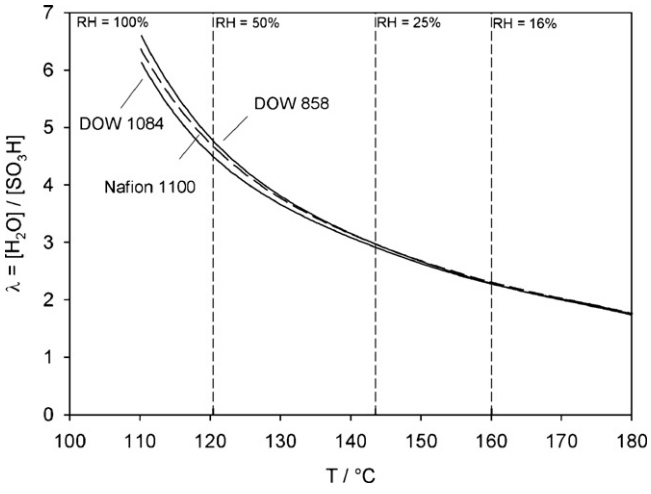

Fig. 8. Water uptake of Dow 858, Dow 1084 and Nafion 1100 at a fixed water pressure of $p_{H_2O} = 10^5$ Pa (1 atm) (hydration isobar).

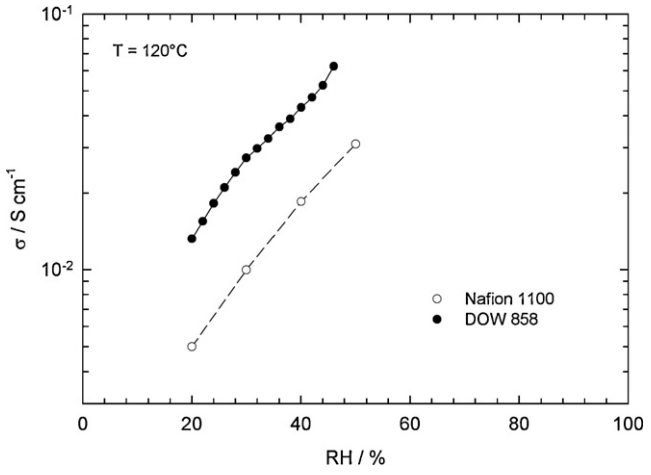

Fig. 9. Proton conductivity of Dow 858 and Nafion 1100 as a function of relative humidity RH at $T = 80\,^{\circ}C$.

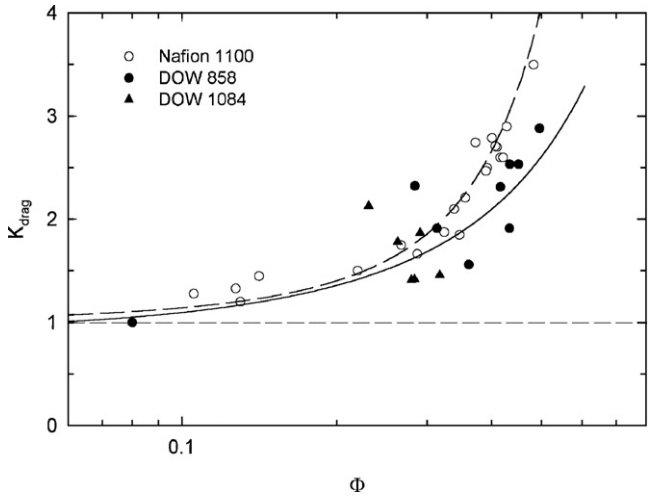

Fig. 10. Room temperature electroosmotic water drag coefficients measured by the E-NMR technique for Dow 858, Dow 1078 and Nafion 1100. The data are plotted as a function of the water volume fraction φ; all data virtually fall onto one curve for a plot versus $\lambda = [H_2O]/[-SO_3H]$ (not shown).

very low degrees of hydration. This effect is also confirmed at $T = 120\,^{\circ}C$, where the conductivity of Dow 858 is more than two times higher than this of Nafion 1100 in the relative humidity range RH = 20–50% (Fig. 9). This actually suggests different changes of the microstructures with temperature and decreasing degree of hydration for both types of ionomer. It should be mentioned at this point that this regime falls right within the α-relaxation of Nafion which recently has been assigned to the onset of long-range chain/side-chain mobility as a result of the destabilization of the electrostatic network [20,21], which occurs at a somewhat higher temperature for the Dow membranes, as will be discussed later. These transitions may allow for conformational changes especially in the presence of pressure [22], which are also expected to affect the proton conductivity (note, that conductivities have been recorded by the two point method, which always requires the application of some pressure to the electrodes to ensure good electrical contact).

But before further discussing the changes occurring in the high temperature regime, let us first continue the discussion of the transport coefficients by considering the coupling of water and proton transport (i.e. electroosmotic drag). The room temperature electroosmotic water drag coefficient, K, i.e. the number of water molecules "dragged" through the ionomer per protonic charge carrier, are shown in Fig. 10 for Dow 858, Dow 1084 and Nafion 1100. The data for Dow 1084 are restricted to water volume fractions less than 30% because this morphologically stable ionomer is difficult to swell beyond this limit. But the few data are close to the drag coefficients measured for Nafion 1100. This is not surprising considering the similar degrees of hydrophobic/hydrophilic separation (Fig. 3) and the virtually identical ion exchange capacities. These two parameters are generally considered to determine electroosmotic drag, which has a high hydrodynamic contribution especially at high degrees of hydration [17]. For Dow 858, the ionomer with the highest IEC, the electroosmotic drag is slightly lower than for the other two ionomers for a given water volume fraction (Fig. 10). The fact that the drag coefficients virtually coincide when plotted as a function of λ suggests that the slight differences are mainly determined by the interaction of the water with different numbers of sulfonic acid groups. With respect to applications in fuel cells, it should be mentioned that the water uptake in terms of λ is similar for all three ionomers (Fig. 1), i.e. for a given relative humidity the electroosmotic water drag coefficients are similar, but the proton conductivity of Dow 858 is about 50% higher than that of the other two ionomers.

Returning to the visco-elastic instabilities, let us next consider the elastic modulus as a function of temperature (Fig. 11). In accordance with the generally observed higher morphological stability of SSC ionomers (e.g. Refs. [4–7]), the strong decrease in the elastic modulus occurs at about 25–35 °C higher temperatures than for Nafion. This decrease corresponds to the α-relaxation observed in tan δ determined from DMA measurements [20,21], i.e. the onset of structural instabilities allowing for irreversible changes in the conformation of the polymer. Whether such changes actually occur and whether these changes

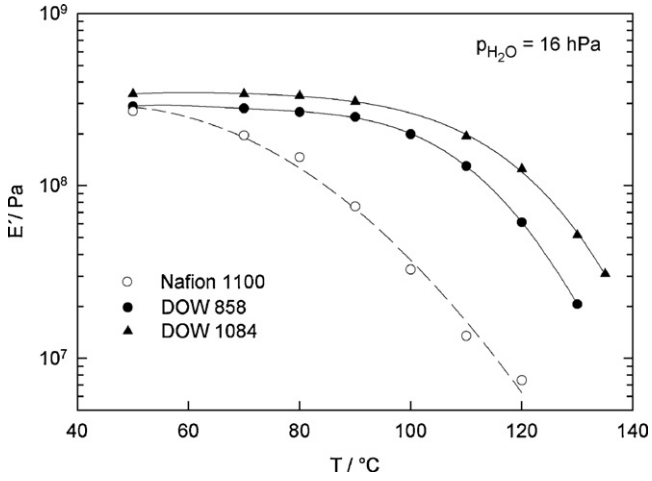

Fig. 11. Real part of the elastic modulus E' obtained by DMA for Dow 858, Dow 1084 and Nafion 1100 as a function of temperature and a constant water pressure of $p_{H_2O} = 16$ hPa (mbar) (note that this corresponds to a decreasing relative humidity with increasing temperature).

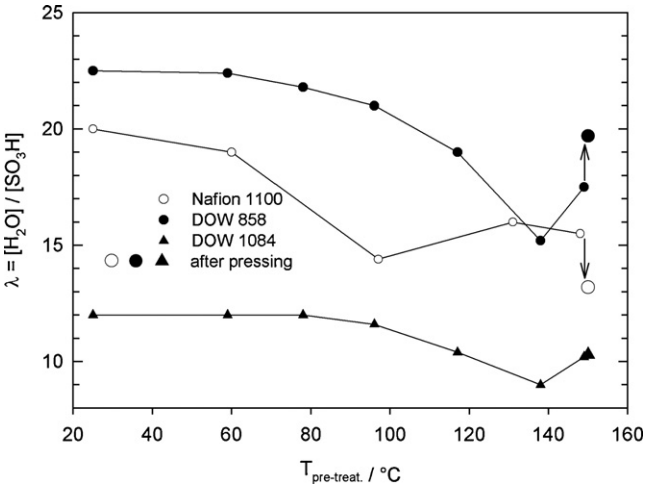

Fig. 12. Water uptake of Dow 858, Dow 1084 and Nafion 1100 at room temperature, after pre-treatment at the given temperature $T_{\text{pre-treat}}$ in a nitrogen atmosphere with a water partial pressure of $p_{H_2O} = 17$ hPa (mbar). Wet membranes were also pressed ($p = 130$ MPa) at $T = 150\,^{\circ}C$ for 30 min before measuring the swelling at room temperature.

may affect the ionomer's ability to take up water, has been investigated by annealing free standing films at high temperatures and controlled humidification and by applying pressure to wet membranes at $T = 150\,^{\circ}C$.

The water uptake at room temperature after pre-treatment is shown in Fig. 12. Indeed, for all three membranes, the swelling at room temperature (and of course also the proton conductivity) is progressively reduced with increasing annealing temperature. The similarity of the temperature dependence to that of the elastic modulus (Fig. 10) is consistent with conformational changes being the main reason for the decreasing swelling compared to membranes preconditioned in water at $T = 60\,^{\circ}C$ (see Section 2). It should be noted that the observed changes might additionally be due to the substantially reduced hydration number λ under the conditions of the pre-treatment. This may drop well below $\lambda = 1$, where a sudden decay of the elastic modulus has been reported [23]. A further decrease of the water uptake capability is observed after the applications of pressure (Fig. 12), and the pronounced dependence on the time of the treatment points to a kind of tixotropic behavior, i.e. extremely slow changes. For the SSC membranes, the onset of these changes occurs at somewhat higher temperatures than for Nafion 1100.

3.2. Implications for the performance in fuel cells

In this section we discuss the implications of the results presented above on the membrane properties under fuel cell operating conditions, in particular for DMFCs and PEM fuel cells operating at higher temperatures. This discussion is exclusively based on the results of simulations making use of the transport and hydration data presented above. The underlying physical chemical model takes into account the fact that the major force driving water into the membrane is entropic (osmosis). As a result of this, any water concentration gradient also corresponds to a gradient in osmotic pressure, especially at high degrees of hydration. The analysis of transport coefficients clearly demonstrated, that these pressure gradients must not only be included as an extra term into the gradient of the chemical potentials, $\tilde{\mu}_i = \mu_i^o + RT \ln a_i + V_i^m p + nF\Phi$, but also as a separate driving force ∇p into the transport equation, which writes in its general form as: $\begin{pmatrix} \vec{j}_{H^+} \\ \vec{j}_{H_2O} \\ \vec{j}_{\text{hydro}} \end{pmatrix} = L_{ij} \begin{pmatrix} \nabla\tilde{\mu}_{H^+} \\ \nabla\tilde{\mu}_{H_2O} \\ \nabla p \end{pmatrix}$ [17]. The reason for this is that, apart from chemical diffusion processes, there is also a contribution from hydrodynamic transport (i.e. viscous flow), $\vec{j}_{\text{hydro}}$, which dominates the transport of water at high degrees of hydration. The transport coefficients L_{ij} used in the simulations are actually obtained from conductivity data, water diffusion coefficients, permeation diffusion coefficients, ion exchange capacities and thermodynamic data (hydration isotherms) presented in this work and Ref. [17]. The key expression of the model is the total water flux, which may be written as:

$$\vec{j}_{H_2O} = \vec{j}^{\text{diff}}_{H_2O} + \vec{j}^{\text{hydro}}_{H_2O} = K_{\text{drag}} \vec{j}_{H^+} + RT \left(\frac{P_{H_2O}}{V^m_{H_2O}} + \frac{K_{\text{drag}}\sigma}{F^2} \right) \frac{\nabla c_{H_2O}}{c_{H_2O}}$$

where K_{drag} and p_{H_2O} are the electroosmotic drag and the water permeation coefficient, respectively. It is worth noting that both transport coefficients describe a combination of both diffusion and viscous flow, and this is the reason why the total water flux is written in such a relatively simple way. Details of the simulation scheme will be published in a forthcoming paper [24].

For Dow 858, Dow 1084 and Nafion 1100 all model parameters are available except for permeation diffusion coefficients at high water contents which are only available for Nafion 1100 [17]. For the present simulations, we have therefore used the permeation diffusion coefficients of Nafion for the Dow membranes. At this stage, this is probably a reasonable approximation considering the fact that the water self-diffusion coefficients are virtually identical for all three membranes within this hydration range (Fig. 4a).

3.3. Membranes under DMFC conditions

The first set of simulations was actually carried out in an attempt to obtain information on the total solvent (water, methanol) cross-over in DMFCs. On the anode side, the membranes were assumed to be in equilibrium with an aqueous solution of methanol. Since the methanol molarity is typically very low (i.e. <2 M), we have simply assumed the solvent uptake to be identical to this in pure water, i.e. $\lambda = 12$, 20 and 22 for Dow 1084, Nafion 1100 and Dow 858, respectively, and the electroosmotic drag being identical for water and methanol, which already has been proven for the case of Nafion [25]. In order to represent different air flows in the cathode structure, the local hydration at the membrane/cathode interface was set to values ranging from $\lambda = 5$ (dry) to a value a little higher, where condensation occurs (wet), i.e. the cathode structure may be subjected to flooding.

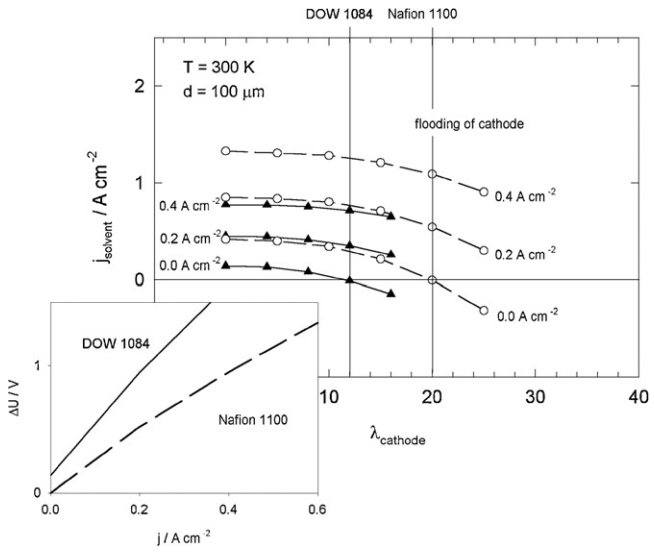

Fig. 13. Simulation results of room temperature membrane properties under DMFC conditions (see text) for Dow 1084 and Nafion 1100 (thickness = 100 μm). Total solvent (water and methanol) cross-over ($j_{solvent}$) as a function of current density and hydration level λ at the cathode side; the range where flooding of the cathode structure is expected is indicated. The insert shows the potential drops as a function of the current density. Note that there is still some cross-over at zero current densities and $\lambda_{cathode}$ below the dew point of water.

Fig. 13 actually shows the total solvent (water, methanol) cross-over from the anode to the cathode for a Dow 1084 or Nafion 1100 membrane with thickness of 100 μm. As expected, there is some cross-over even when no current is drawn from the cell as long as there is some solvation gradient across the membranes. This is due to solvent permeation and diffusion, which is about a factor of three lower for Dow 1084 compared to Nafion 1100. This factor is actually reflected in the increase of water permeation and diffusion when going from λ = 12 (Dow 1084) to λ = 20 (Nafion 1100), i.e. the lower cross-over at zero current is just the consequence of the lower swelling of Dow 1084 compared to Nafion 1100.

Also in the presence of a current across the membranes, the cross-over remains lower for Dow 1084 compared to Nafion 1100, however, by a factor lower than two at high current density (Fig. 13). Under these conditions, cross-over is mainly determined by electroosmotic drag, which is virtually identical for both membranes and a given degree of hydration (Fig. 10). Therefore, the reduced cross-over under load is just the result of the lower swelling of Dow 1084. Of course, the price to pay for this lower cross-over is the higher membrane resistance, i.e. a higher potential loss (ΔU) which is shown in the insert of Fig. 13. This is less than a factor of two higher than for the Dow membrane at current densities where the solvent cross-over is lower by about the same factor.

In short, the reduced swelling of Dow 1084 compared to Nafion 1100 leads to a significantly lower cross-over at zero current density (factor of three), while, under load, the reduced cross-over is achieved at the expense of a reduction in proton conductivity. As expected, simulations of the properties of thinner membranes show higher cross-over under open-circuit conditions, but similar cross-over under load, where the lower membrane resistances lead to lower potential losses. Therefore, thick membranes are preferred for low current density applications or applications with long stand-by periods, while thinner membranes may be chosen for DMFCs operating at high current densities. For the latter application, it may even be useful to use Dow 858 membranes. Because of their high swelling at the cathode side (λ = 22) and the high IEC, the potential drop across the membrane is reduced by almost 40% while the electroosmotic water drag governing the cross-over at high current density is only slightly higher than for Nafion 1100 under the same conditions (Fig. 10). The same is true for the cross-over at zero current density.

3.4. Membrane properties under PEM fuel cell conditions

For the application of membranes in PEM fuel cells operating with hydrogen or a hydrogen-rich reformate as a fuel, the membrane resistance and the corresponding potential drop across the membrane is an important datum. Another feature is the mechanical stability which is important for maintaining the optimized morphology of the membrane/electrode interfaces.

Simulations have been carried out for Dow 858 and Nafion 1100 membranes of a thickness of $d = 20\,\mu m$ and no water desorption at the membrane/cathode interface, i.e. the best self-humidifying conditions for the membranes. For the anode gas a relative humidity of RH = 95% has been chosen for temperatures up to $T = 80\,^{\circ}C$. Above this temperature, the water partial pressure is set to $p_{H_2O} = 500\,hPa$ (mbar), i.e. decreasing relative humidity with increasing temperature, which is assumed to be close to conditions within operating fuel cells. The water desorption/absorption coefficient describing the water transfer through the anode/membrane interface has been set to a value ($K = 10^{19}\,s^{-1}\,cm^{-2}$) which corresponds to medium hydrophilicity.

The different behavior of Dow 858 and Nafion 1100 membranes may be illustrated by considering the steady state water profiles obtained for $T = 80\,^{\circ}C$ as a function of the current density. These are shown in Fig. 14a in terms of water volume fractions across the membrane. Apparently, the water profiles are generally flatter for the Dow membrane, i.e. the anode side is less dried out while the cathode side shows similar degrees of hydration for both type of membranes (Fig. 14a). The reason for this difference is essentially the slightly lower electroosmotic drag for Dow 858 compared to Nafion 1100 for a given water volume fraction (see Fig. 10). In the case of the Nafion 1100 membranes, two competing effects show up in the evolution of the water profiles: changing the current density from $j = 0.2\,A\,cm^{-2}$ to $j = 0.4\,A\,cm^{-2}$ is actually increasing the degree of self-humidification, while the further increase of the current density to $j = 0.6\,A\,cm^{-2}$ is leading to the onset of membrane drying at the anode side. This complex behavior is the result of the interplay of water permeation (from the cathode to the anode) and the electroosmotic water drag (from the anode to the cathode), and it is sensitive to the water desorption/absorption properties (hydrophilicity) at the membrane/anode interface.

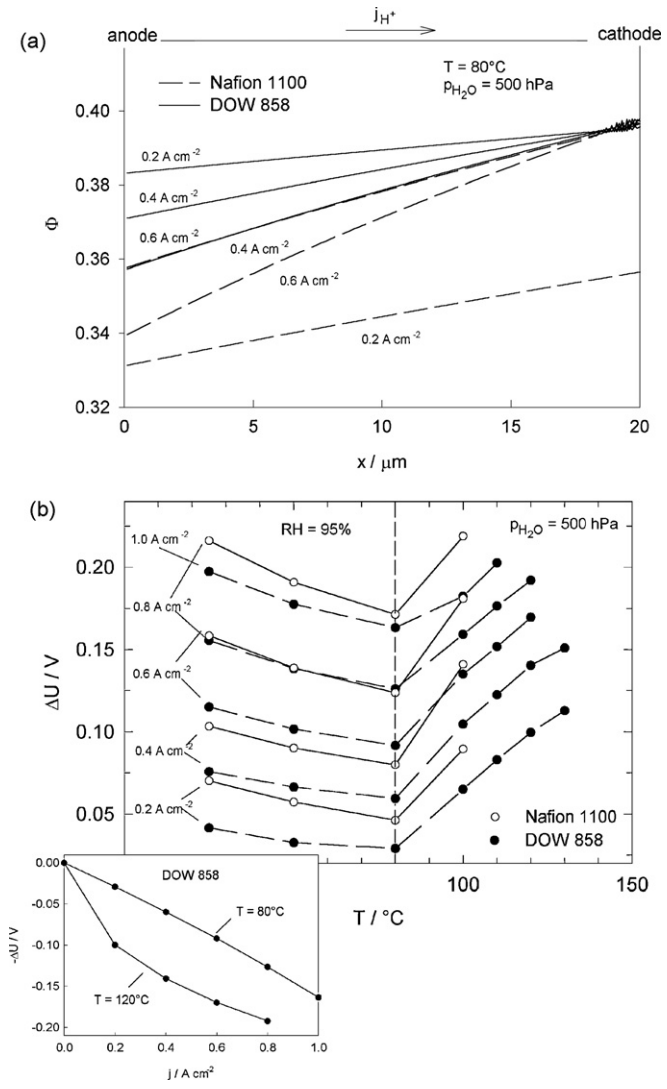

Fig. 14. A few results of simulations of membrane properties under PEM fuel cell conditions (see text) for Dow 858 and Nafion 1100 (thickness = 20 μm). Note, that the water desorption at the cathode side is set to zero corresponding to optimum self-humidifying conditions. (a) Water distribution along the current for different current densities. (b) Voltage drop across the membrane as a function of temperature for different current densities. For temperatures below $T = 80\,^{\circ}C$, the relative humidity at the anode side is set to RH = 95%; for temperatures above $T = 80\,^{\circ}C$, a constant water partial pressure ($p_{H_2O} = 500$ hPa) is used for the simulations. Note that the simulations have been carried out up to temperatures where the elastic moduli are about 10% of the elastic moduli at room temperature (see Fig. 11 and text).

The resulting potential losses across the membranes are significantly lower for Dow 858 compared to Nafion 1100 (Fig. 14b). To some extend, this is because of the higher hydration (especially at the anode side) leading to higher proton mobilities D_σ (Fig. 5), but the major reason is simply the higher IEC of Dow 858, i.e. the higher charge carrier concentration. The potential loss across the Dow 858 membrane is actually lower for all simulated operation conditions (Fig. 14b). The self-humidification effect which is seen in the Nafion water profiles at $T = 80\,^{\circ}C$ (see above) is also visible in the potential loss as a function of current density across the Dow membrane at higher temperatures (insert in Fig. 14b). While the potential decreases in an almost linear fashion at $T = 80\,^{\circ}C$, which reflects only minor dehydration with increasing current density, the potential drop at $T = 120\,^{\circ}C$ sharply increases with current at low current density before it tends to level off as a result of progressive self-humidification with increasing current density.

The simulations for Nafion 1100 were only carried out for temperatures up to $T = 100\,^{\circ}C$ where proton conductivity is already a strong function of the membrane history (time, humidification, strain). This may simply reflect changes in the membrane properties, which are probably the result of the dramatically changing mechanical properties in this temperature regime (see also Fig. 11). Apart from the decreasing capability to absorb water (Fig. 12), the severe softening of Nafion 1100 may lead to morphological changes of the membrane/electrode interfaces, which definitely gives rise to additional potential losses.

Obviously, Dow 858 membranes have the potential to perform better within a wide range of operation conditions. As for DMFCs (see above), this has mainly to do with the higher IEC and the lower electroosmotic drag under operating conditions. In a DMFC the latter is just the consequence of the lower hydration of Dow 1084 compared to Nafion 1100. In a PEM fuel cell, however, this is the result of the lower electroosmotic drag of Dow 858 compared to Nafion 1100 for a given water volume fraction. It should be noted that the hydration of Dow 858 is higher than the hydration of Nafion 1100 in terms of water volume fraction (Fig. 14a), but lower in terms of hydration numbers under these conditions.

4. Conclusions and outlook

No distinct differences in water and proton transport and in the hydrophobic/hydrophilic separation as a function of water volume fraction were observed for SSC PFSA ionomers (Dow) compared to Nafion of the same equivalent weight. The significantly higher elastic modulus of Dow may be the sole reason for its superior performance as the electrolyte in a fuel cell. The better mechanical properties allow for the formation of membranes with higher IEC (lower equivalent weight) which leads to an increased concentration of protonic charge carriers and a reduction in hydrophobic/hydrophilic separation.

The reduced swelling of the Dow membranes of similar equivalent weight when used in DMFCs reduces solvent (i.e. water and/or methanol) cross-over, especially under zero current conditions. Under load, reduced cross-over is accompanied by an increase in voltage drop across the membrane. Dow membranes of lower EW show similar electroosmotic drag coefficients but significantly higher proton conductivity than Nafion, i.e. such membranes are anticipated to show better performance (lower electrical losses) with similar methanol cross-over (chemical losses) when operated at high current density. Some methanol rejection may occur provided higher IEC membranes are developed. This rather surprising phenomenon has already been witnessed in extremely high IEC poly(arylene sulfones) [26] and may lead to further decreases in methanol cross-over when utilized in DMFCs.

The better performance of low equivalent weight SSC membranes in hydrogen fuel cells is chiefly the result of the higher IEC and more effective solvent permeation from the cathode to the anode side in the opposite direction of the electroosmotic drag.

The better morphological stability of SSC membranes compared to Nafion is anticipated to be in favor of the morphological stability of the membrane electrode interfaces. The microstructure of these interfaces is generally optimized, and any morphological change is critical to the performance of both DMFCs [27] and hydrogen fuel cells [28,29]. The higher glass transition temperature of SSC ionomers gives stability to the active layers (i.e. electrolyte/electrode interface) especially at high operation temperatures, where Nafion seems to undergo severe conformational changes.

The present comparison demonstrates that combining high IEC and high mechanical stability (i.e. elastic modulus), e.g. by increasing crystallinity as in the present case, or by increasing molecular weight, cross-linking or introducing interacting particles, is a promising approach to improve membrane performance in both direct methanol and PEM fuel cells.

Acknowledgements

The authors thank H. Steininger (BASF Fuel Cell) for proof reading and the *Bundesministerium für Bildung und Forschung* (project DryD under the contract no. 0329567), and the *Stiftung Energieforschung Baden-Württemberg* (A 23305) for financial support.

References

[1] K. Prater, J. Power Sources 29 (1990) 239–250.
[2] V. Arcella, A. Ghielmi, G. Tommasi, Ann. NY Acad. Sci. 984 (2003) 226–244.
[3] A. Ghielmi, P. Vaccarono, C. Troglia, V. Arcella, J. Power Sources 145 (2005) 108–115.
[4] M.R. Tant, K.D. Lee, K.P. Darst, C.W. Martin, Polym. Mat. Sci. Eng. 58 (1988) 1074–1078.
[5] M.R. Tant, K.P. Darst, K.D. Lee, C.W. Martin, Multiphase polymers: blends and ionomers, in: L.A. Utracki, R.A. Weiss (Eds.), ACS Symposium Series 395, ACS, Washington, 1989, pp. 370–400.
[6] R.B. Moore, C.W. Martin, Macromolecules 22 (1989) 3594–3599.
[7] G.A. Eisman, Proc. 168th Electrochemical Society Meeting 83–13, 1986, pp. 156–171.
[8] G.A. Eisman, J. Power Sources 29 (1990) 389–398.
[9] S.J. Paddison, J.A. Elliott, J. Phys. Chem. A 109 (2005) 7583–7593.
[10] S.J. Paddison, J.A. Elliott, Phys. Chem. Chem. Phys. 8 (2006) 2193–2203.
[11] S.J. Paddison, J.A. Elliott, Solid State Ionics 177 (2006) 2385–2390.
[12] S.J. Paddison, J.A. Elliott, Solid State Ionics 178 (2007) 561–567.
[13] L.B. Shaffer, R.W. Hendricks, J. Appl. Cryst. 7 (1974) 159–163.
[14] T. Dippel, K.D. Kreuer, M. Hampele, A. Rabenau, Recent developments on the pulsed field gradient NMR technique for self diffusion coefficient measurements on various nuclei, in: Proceedings of XXV Congress Ampère, Stuttgart, 1990.
[15] M. Ise, K.D. Kreuer, J. Maier, Solid State Ionics 125 (1999) 213–223.
[16] K.D. Kreuer, J. Membr. Sci. 185 (2001) 29–39.
[17] K.D. Kreuer, S.J. Paddison, E. Spohr, M. Schuster, Chem. Rev. 104 (2004) 4637–4678.
[18] M. Schuster, K.D. Kreuer, H.T. Andersen, J. Maier, Macromolecules 40 (2007) 598–607.
[19] K.D. Kreuer, W. Weppner, A. Rabenau, Solid State Ionics 3/4 (1981) 353–358.
[20] K.A. Page, K.M. Kable, R.B. Moore, Macromolecules 38 (2005) 6472–6484.
[21] K.A. Page, F.A. Landis, A.K. Phillips, R.B. Moore, Macromolecules 39 (2006) 3939–3946.
[22] M. Casciola, G. Alberti, M. Sganappa, R. Narducci, J. Power Sources 162 (2006) 141–145.
[23] F. Bauer, M. Willert-Porada, Solid State Ionics 177 (2006) 2391–2396.
[24] K.D. Kreuer, in press.
[25] K.D. Kreuer, Hydrocarbon membranes, in: W. Vielstich, A. Lamm, H.A. Gasteiger (Eds.), Handbook of Fuel Cells—Fundamentals, Technology and Applications, John Wiley & Sons, Ltd., Chichester, 2003, pp. 420–435.
[26] V. Saarinen, K.D. Kreuer, M. Schuster, R. Merkle, J. Maier, Solid State Ionics 178 (2007) 533–537.
[27] X. Chen, C. Peng, M.D. You, L. Liu, Y. Zang, Q.B. Fan, Electrochim. Acta 51 (2006) 4620–4625.
[28] J. Xie, D.L. Wood, K.L. Moore, P. Atanassov, R.L. Borup, J. Electrochem. Soc. 152 (2005) A1011–A1020.
[29] X.Y. Huang, R. Solasi, Y. Zou, M. Feshler, K. Reifsnider, D. Condit, S. Burlatsky, T. Madden, J. Poly. Sci. B-Poly. Phys. 44 (2006) 2346–2357.